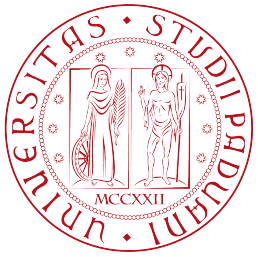

UNIVERSITÀ DEGLI STUDI DI PADOVA

Dipartimento di Fisica e Astronomia "Galileo Galilei"

Corso di Laurea in Fisica

Tesi di Laurea

Development of an electrostatic diagnostic for space charge characterization in a negative ion beam

Relatore

Dott. Gianluigi Serianni

Correlatore

Dott. Emanuele Sartori

Laureando

Valeria Candeloro

Anno Accademico 2017/2018

Abstract

Neutral beam injectors are one of the most applied techniques for plasma heating. Fast neutral beams are unaffected by electromagnetic fields so they can travel for long distances: once they reach the plasma region they are ionized because of collisions and they heat the already existing plasma particles until they reach thermal equilibrium.

These neutral beams are obtained through charge exchange and neutralization of high energy ion beams, which are usually made of positive hydrogen ions H^+ *or negative hydrogen ions* H^-*. The employment of ion beams is technically complex because both positive and negative ions tend to repel each other while propagating.*

Negative ions injectors are more efficient since the H^- *neutralization rate is higher because their additional electrons are weakly tied. On the other hand, these ions are more difficult to produce than positive ions and are easily lost during the acceleration process because of neutralization. However, when the background gas is ionized, positive ions are generated and they are kept into the beam region, which has a lower potential. This phenomenon is known as space charge compensation and it allows the beam to propagate for longer distances.*

The aim of this thesis work is the spatial charge characterization of the H^- *beam in NIO1, a negative-ions accelerator hosted at Consorzio RFX in Padova, through a single Langmuir probe. A better understanding of space charge compensation will be useful with a view to develop highly efficient beam injectors for the ITER reactor.*

Sommario

Gli iniettori di particelle neutre sono tra i metodi più diffusi per il riscaldamento di un plasma. Questi fasci non sono influenzati dai campi elettromagnetici, per cui possono viaggiare per grandi distanze: una volta raggiunto il plasma, le particelle neutre sono ionizzate a causa delle collisioni e riscaldano il plasma stesso trasferendogli la propria energia cinetica, finché non viene raggiunto l'equilibrio termico.

I fasci di particelle neutre possono essere ottenuti tramite la neutralizzazione di fasci di ioni ad alta energia. Nella maggioranza dei casi si utilizzano ioni idrogeno, H^+ *o* H^-*. L'utilizzo dei fasci di ioni è tecnicamente complesso perché in entrambi i casi gli ioni tendono a respingersi tra loro, causando la dispersione del fascio durante la propagazione.*

Gli iniettori di ioni negativi sono più efficienti perché il tasso di neutralizzazione degli H^- *è più alto rispetto a quello degli* H^+*, poiché il loro elettrone addizionale è debolmente legato e, di conseguenza, viene perso facilmente. D'altra parte, gli ioni negativi sono più difficili da produrre rispetto agli ioni positivi e si disperdono facilmente durante il processo di accelerazione proprio a causa dell'elevato tasso di neutralizzazione. Ad ogni modo, quando il gas di background è ionizzato, gli ioni positivi generati sono confinati nella regione del fascio, che ha potenziale minore. Questo fenomeno di compensazione spaziale di carica permette al fascio di propagarsi per distanze maggiori.*

L'obiettivo di questa tesi è la caratterizzazione spaziale di carica del fascio di ioni H^- *prodotto in NIO1, un acceleratore di ioni negativi installato presso il Consorzio RFX (Padova), utilizzando una sonda di Langmuir singola. Una comprensione più profonda del fenomeno di compensazione spaziale di carica sarà utile per la realizzazione di iniettori di neutri altamente efficienti per il reattore a fusione nucleare ITER.*

Contents

Chapter 1

Introduction

1.1 Nuclear fusion

Energy waste and environmental protection are undeniably among the main problems that the world is currently facing: most of the energy is produced from non-renewable sources which have a negative impact on the environment. However, today it is not possible to provide all the energy needed from the currently employed renewable sources.

Nuclear fusion is probably the only option available that may resolve this energy crisis, since it would satisfy the energy consumption while producing neither radioactive waste nor air pollution: in fact, its fuel would be deuterium, a hydrogen isotope which is not dangerous for the environment and it is easily available on Earth. Another great advantage of nuclear fusion is that even in the worst case scenario fusion reactors would not be dangerous for the environment in case of an accident.

1.2 ITER project

The European Union, Japan, Russia, India, China, Korea and the United States are currently co-operating on the ITER[6] project, a nuclear fusion reactor that should be able to produce 500 MW of power from 50 MW of heating power. One of the main technological and scientific challenges is plasma heating: in fact, ITER will contain a deuterium-tritium plasma confined by magnetic fields and requires a hot plasma (around 20 keV) to sustain the fusion reaction for long periods of time.

The most important method for plasma heating is Neutral Beam Injection (NBI). High energy neutral particles can be transported for long distances since they are not influenced by electromagnetic fields, until they collide with the plasma and their kinetic energy heats the plasma itself. NBI usually employs positive ions as H^+ but negative ions NBI are more efficient when high beam energy is required, even if their application is more complex.

The ITER Neutral Beam Test Facility (NBTF) is hosted at Consorzio RFX, in Padova, and it is called PRIMA (Padova Research on ITER Megavolt Accelerator). Two experiments are currently underway, SPIDER and MITICA. SPIDER (Source for Production of Ion of Deuterium Extracted from Rf plasma) is the full-size ITER negative-ions source, while MITICA (Megavolt ITER Injector & Concept Advancement) is the full-scale protoype of the ITER NBI.

1.3 NIO1

NIO1[7] (Negative Ion Optimization phase 1) is a negative-ions accelerator hosted at Consorzio RFX which was installed in order to analyze basic phenomena of the negative ion beam development and to validate numerical models. The experiments on NIO1 will provide a better understanding of this phenomenon that will be useful for both SPIDER and MITICA.
NIO1 device can be divided in three parts: the source, the accelerating column and the diagnostic tube.

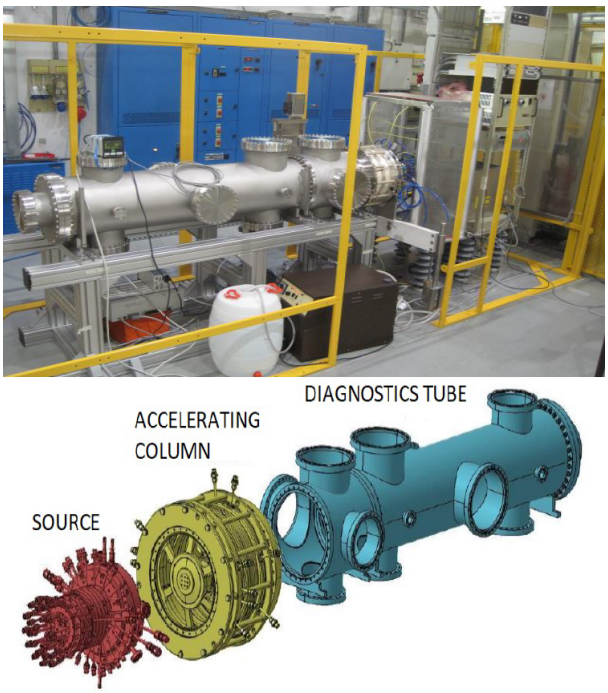

Figure 1.1: NIO1 experiment.

Negative ions are produced in the source and are then accelerated through the column, which is composed by four grids:

- The *Plasma grid* (PG) is in contact with the plasma. Its potential is the actual source acceleration voltage and its maximum value is 60 kV;
- The *Extraction grid* (EG) voltage is higher than the PG voltage, so the ions are accelerated. The acceleration potential in this section is $V_{EG} - V_{PG}$ and its maximum value is 10 kV;
- The *Post-acceleration grid* (PA) is always at ground potential, while the *Repeller grid* is usually held at ground potential or positive voltage and it restrains the positive ions that otherwise would be accelerated back into the plasma.

The extracted beam is composed by 9 single beamlets arranged in a 3×3 matrix.

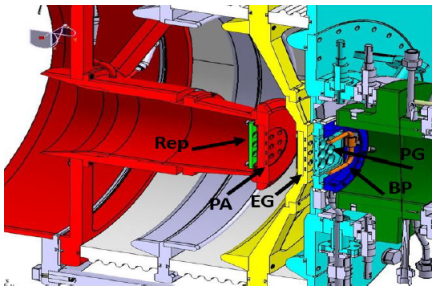

Figure 1.2: Accelerated column schematics.

The diagnostic tube is a 1.5 m long tube with 350 mm inner radius. It houses several beam diagnostics which can be used in order to characterize the ion beam.

The main problem of negative ion sources is beam collimation: negative ions tend to repel each other after being accelerated and, as a consequence, the beam is dispersed. The ITER injector requires 1 MeV of beam energy and 40 A of extracted current: in these conditions space charge density is very high and this problem might be counterproductive.
However, as the beam propagates in the background gas a lot of positive ions are produced from ionization and the system potential can even become positive because of partial charge compensation. This phenomenon counteracts the beam dispersion, keeping it collimated.

The aim of this work is to analyze space charge compensation in NIO1 through a single Langmuir probe installed in the diagnostic tube, at a distance of approximately 0.5 m from the accelerating column. If polarized with respect to the plasma, the Langmuir probe collects current: the analysis of the I-V characteristic curve provides useful information such as ion densities and temperatures.

The beam-background gas interaction will also be investigated in two different experimental conditions, with and without an additional cryogenic pump.

Chapter 2

Current collection model

A single Langmuir probe is essentially made of one electrode exposed to the plasma which collects current when polarized with respect to the plasma. When the bias between the probe potential and the plasma potential is not zero, a sheath is formed in the region that surrounds the probe surface: if the bias is negative, this region is characterized by a negative space charge density which favors the ion current collection. On the other hand, if the bias is positive the electron current collection will then be favored.
This chapter provides a theoretical model of current collection for a single Langmuir probe, including the sheath effect.

2.1 Probe current

After being produced in the source, negative ions are accelerated and propagate within the background gas, which is molecular hydrogen H_2. The interaction causes gas ionization, so positive ions and electrons are produced and consequently the plasma is created.

In NIO1 the beam injection is made of negative hydrogen ions H^-. The beam development will be investigated after passing through the acceleration column, so the electrons generated because of secondary emission or electron stripping inside the accelerator are neglected since they are drifted by the permanent magnets on the post-acceleration grid.
Some positive ions H^+ and neutral atoms H^0 are also produced inside the accelerating column, but their energy is lower than the initial beam energy and the H^+ ions are retarded by the electric fields. However, some of them can actually reach the diagnostic tube if their kinetic energy is sufficiently high.

The ionization process is described by the following reactions[8]:

$$\begin{aligned} H^- + H_2 &\rightarrow H^- + H_2^+ + e^- \\ H^0 + H_2 &\rightarrow H^0 + H_2^+ + e^- \\ H^+ + H_2 &\rightarrow H^+ + H_2^+ + e^- \end{aligned}$$

Plasma ions and electrons usually are the largest contributions for the probe current. However, other phenomena such as electron stripping and secondary electron emission can produce additional electrons inside the diagnostic tube so they must be taken into account, otherwise it is not possible to correctly describe the I-V characteristics.

The total current is the result of different contributions, which are:

- Beam current, I_{beam};
- Positive ions current, I_+;
- Plasma electrons current, I_-;
- Secondary emission electrons current, I_{see};
- Stripped electrons current, I_{se}.

Each term will be described individually in the following sections.

2.1.1 Beam current

The beam current I_{beam} is the effective quantity of extracted current that reaches the probe. Previous studies [1] on NIO1 have shown how the beam composition changes at different distances from the extraction grid.

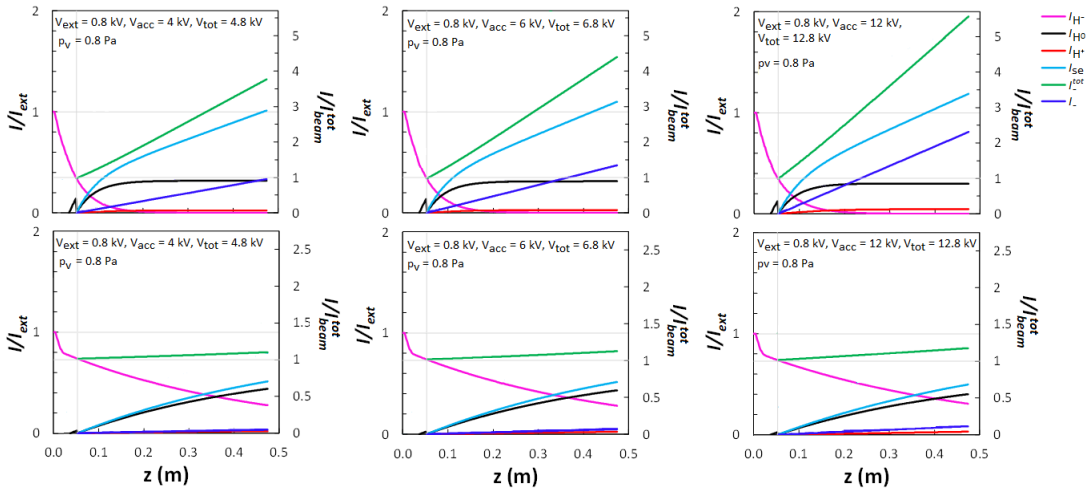

Figure 2.1: Beam composition along its axis for different V_{acc}, above without cryopump, below with cryopump. The vertical grey line indicates the end of the accelerating column. I^{tot}_{beam} is the initial beam current (for z = 0.05 m), I_{ext} is the extracted current form the source, $V_{\text{ext}} = V_{\text{EG}} - V_{\text{PG}}$, $V_{\text{acc}} = V_{\text{EG}} - V_{\text{PA}}$, $V_{\text{tot}} = V_{\text{PG}} - V_{\text{PA}}$, p_{v} is the vessel pressure.

According to Figure 2.1, if the cryopump is not operating the measured negative current I^{tot}_{-} is three times larger than the total beam current I^{tot}_{beam} when z = 0.5 m. At this distance from the source the H^- current is almost zero and the beam is mainly composed of neutral particles H^0 and a small amount of positive ions H^+:

$$I_{\text{H}^0} = 0.9 I^{tot}_{\text{beam}}$$
$$I_{\text{H}^+} = 0.1 I^{tot}_{\text{beam}}$$

On the other hand, if the cryopump is working $I^{tot}_{-} \sim 1.1 I^{tot}_{\text{beam}}$ when z = 0.5 m and at this distance the beam is almost equally divided into H^- and H^0:

$$I_{\text{H}^0} = 0.55 I^{tot}_{\text{beam}}$$
$$I_{\text{H}^+} = 0.45 I^{tot}_{\text{beam}}$$

The general expression for the collected beam current is:

$$I_{\text{beam}} = \frac{I_{\text{H}^-} - I_{\text{H}^+}}{A_{\text{beam}}} dl \tag{2.1}$$

where I_{H^-} and I_{H^+} have different values depending on whether the cryopump is working or not, $d = 2.4$ mm is the probe diameter, $l = 15$ mm is the probe length and $A_{\text{beam}} = 0.016$ m^2 is the beam area. In this case the probe collecting surface is assumed to be equal to the geometrical probe surface since the beam is not affected by orbital effects (see Appendix A).

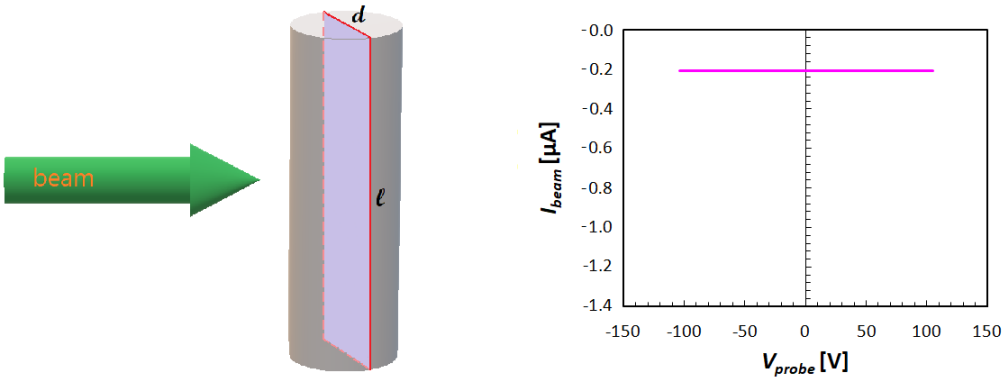

Figure 2.2: Example of collected beam current when the cryopump is not working.

2.1.2 Positive ion current

Positive ions are collected if the probe potential is lower than the plasma potential. In this case I_+ is defined as follows:

$$I_+ = eS^+_{\text{eff}} n_{\text{i,s}} u^*_{\text{Bohm}} \tag{2.2}$$

where e is the elementary charge, S^+_{eff} is the effective probe collecting surface and $n_{\text{i,s}}$ is the H_2^+ spatial density at the sheath edge and u^*_{Bohm} is the modified Bohm velocity, the expression of which is explained in detail in Appendix C. The ion density at sheath edge is somewhat reduced by a factor h_{r}, defined as *edge-to-center density ratio*, with respect of the density in the plasma bulk $n_{\text{i,0}}$, and therefore $n_{mathrmi,s} = h_{\text{r}} n_{\text{i,0}}$.

Otherwise, if the probe potential is greater than the plasma potential, the ions are repelled from the probe and the current equation is:

$$I_+ = eA_{\text{probe}} n_{\text{i,s}} u^*_{\text{Bohm}} e^{-\frac{V - V_{\text{P}}}{\text{T}_i}} \tag{2.3}$$

where V is the probe potential, V_{P} is the plasma potential, A_{probe} is the geometrical probe surface and T_i is the positive ion temperature in eV.

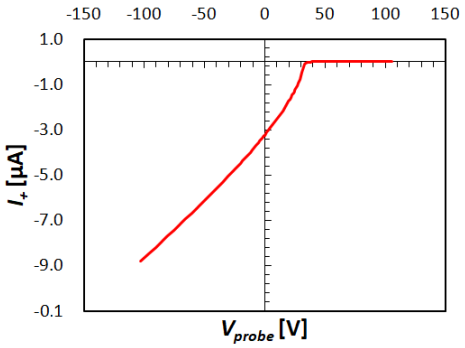

Figure 2.3: I_+ has a linear trend for $V < -50$ V, while it decreases rapidly when $V > V_{\text{P}}$.

The effective probe surface depends on the sheath thickness s which can be estimated with several models, as will be shown in chapter 4.

2.1.3 Plasma electron current

Unlike positive ions, the electrons are repelled if the probe potential is lower than the plasma potential. As shown by P. Chabert in [2], in this case the plasma electron current is defined as follows:

$$I_- = I_{\mathrm{sat},-} e^{\frac{(V-V_\mathrm{P})}{\mathrm{T_e}}} \tag{2.4}$$

where T_e is the electron temperature in eV and $I_{\mathrm{sat},-}$ is the electron saturation current defined as:

$$I_{\mathrm{sat},-} = \frac{1}{4} e n_{e,0} A_{\mathrm{probe}} \bar{v}_{\mathrm{avg}} \tag{2.5}$$

where $\bar{v}_{\mathrm{avg}}$ is the average velocity for a Maxwellian electron distribution given by

$$\bar{v}_{\mathrm{avg}} = \sqrt{\frac{8e\mathrm{T_e}}{\pi m_e}} \tag{2.6}$$

A_{probe} is the probe surface, m_e is the electron mass and $n_{e,0}$ is the plasma electron density at plasma bulk.
On the other hand, if the probe potential is greater than the plasma potential the electrons are collected and the current equation is:

$$I_- = \frac{I_{\mathrm{sat},-}}{A_{\mathrm{probe}}} S^-_{\mathrm{eff}} \tag{2.7}$$

In this case the effective probe collecting surface is obtained with the OML Theory (see Appendix A).

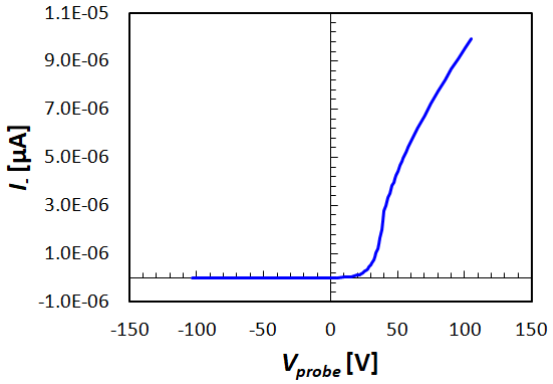

Figure 2.4: I_- has a linear trend for high values of V, while it is negligible for $V < V_\mathrm{P}$.

2.1.4 Secondary electron emission

When the beam interacts with the probe surface some electrons are released from the probe itself. Plasma ions and electrons can also produce secondary emission but their contribution can be neglected because beam ions are much more energetic. This current is seen by the probe as an apparent positive ion current.

As shown by Hershkowitz in [3], if the probe potential is lower than the plasma potential the emitted electrons flow into the plasma and the current expression is:

$$I_{\text{see}} = \frac{(\pi\gamma_{\text{see}} + 1)I_{\text{H}^0} + \pi\gamma_{\text{see}}I_{\text{H}^-}}{A_{\text{beam}}} A_{\text{probe}} \tag{2.8}$$

otherwise if the probe potential is greater than the plasma potential the probe holds back the electrons and the current is defined as:

$$I_{\text{see}} = \frac{(\pi\gamma_{\text{see}} + 1)I_{\text{H}^0} + \pi\gamma_{\text{see}}I_{\text{H}^-}}{A_{\text{beam}}} A_{\text{probe}} e^{-\frac{V-V_p}{\text{T}_{\text{see}}}} \left(1 + \frac{V - V_p}{\text{T}_{\text{see}}}\right)^{\frac{1}{2}} \tag{2.9}$$

where γ_{see} is the *secondary emission coefficient*, a positive number which depends on the probe material characteristics and T_{see} is the emitted electron temperature in eV. The π factor results from integration over the impact angle on a cylindrical geometry and takes account of the angular dependence of secondary electron emission with respect to normal incidence. This is generally assumed to be $\gamma_{\text{see}}^{eff} = \sec(\theta)\gamma_{\text{see}}$, with θ incidence angle with respect to the normal angle.

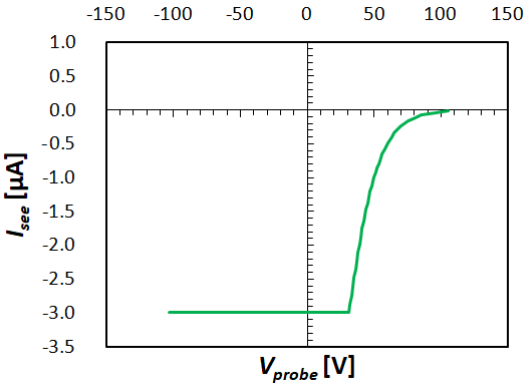

Figure 2.5: I_{see} reaches its maximum value when $V - V_{\text{P}}$ and decreases for higher voltages.

2.1.5 Stripped electrons current

The single and double electron stripping process are described as follows:

$$\text{H}^- + \text{H}_2 \rightarrow \text{H}^0 + \text{H}_2^* + e^-$$
$$\text{H}^0 + \text{H}_2 \rightarrow \text{H}^+ + \text{H}_2^* + e^-$$
$$\text{H}^- + \text{H}_2 \rightarrow \text{H}^+ + \text{H}_2^* + 2e^-$$

This current contribution is then proportional to the total beam current, which includes the neutral atoms H^0:

$$I_{\text{se}} = \alpha_{\text{strip}} \frac{I_{\text{beam}}^{tot}}{A_{\text{beam}}} S_{\text{eff}}^{se} \tag{2.10}$$

where α_{strip} is the *stripping coefficient* and S_{eff}^{se} is the effective collecting surface for stripped electrons, defined as:

$$S_{\text{eff}}^{se} = 2b_{\text{se}}l \tag{2.11}$$

where b_{se} is the impact parameter given by the OML Theory (Appendix A).

The $I_{se} - V$ curve is shown in the next figure:

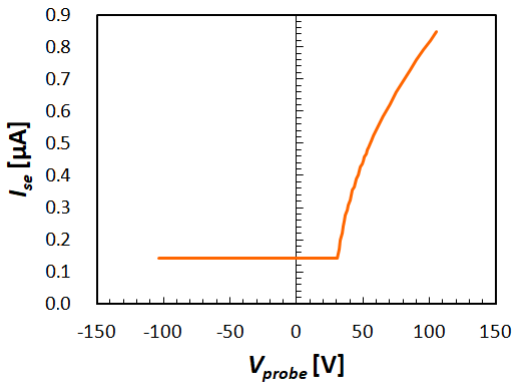

Figure 2.6: I_{se} has a similiar trend to that of I_-, but it is of one order of magnitude smaller.

2.2 Final expression for probe current

The final analytical expression for the total collected current is:

$$I_{probe} = I_{beam} - I_+ + I_- + I_{se} - I_{see} \tag{2.12}$$

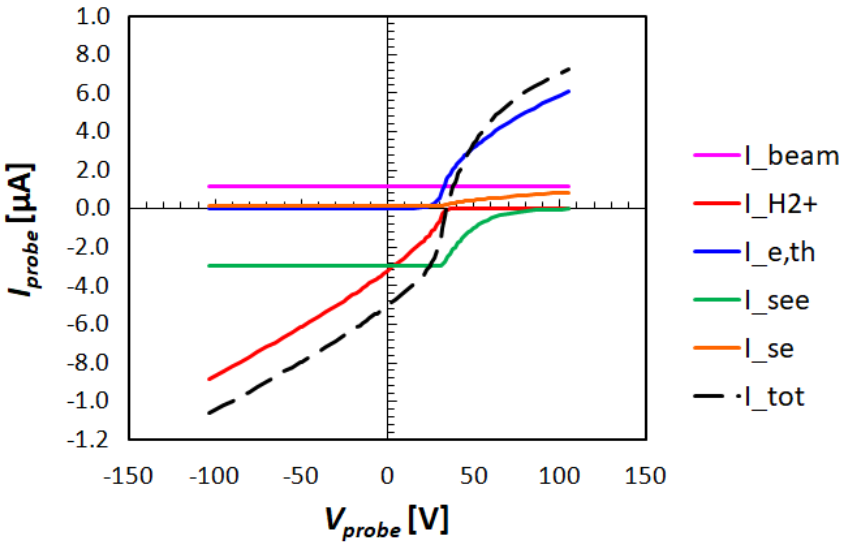

Figure 2.7: I_{probe} with a non negligible negative beam current. The total current is almost completely given by plasma ions and electrons and secondary emitted electrons.

Figure 2.7 shows all contributions with their sign. The beam current I_{beam} can be both positive or negative depending on the beam composition.

The experimental data can be fitted with this function in order to estimate several plasma parameters such as densities, temperatures and the coefficients γ_{see} and α_{strip}.

Chapter 3

Experimental setup and data

3.1 Probe design

The single Langmuir probe used in this experiment is made of a steel stick covered with a pyrex glass tube. The electrode diameter is 2.4 mm and its length is 15 mm. The whole system is fixed on the NIO1 manipulator with vacuum adhesive tape, the electrical contacts are made with clamps and the wires return to the surface passing inside the manipulator.

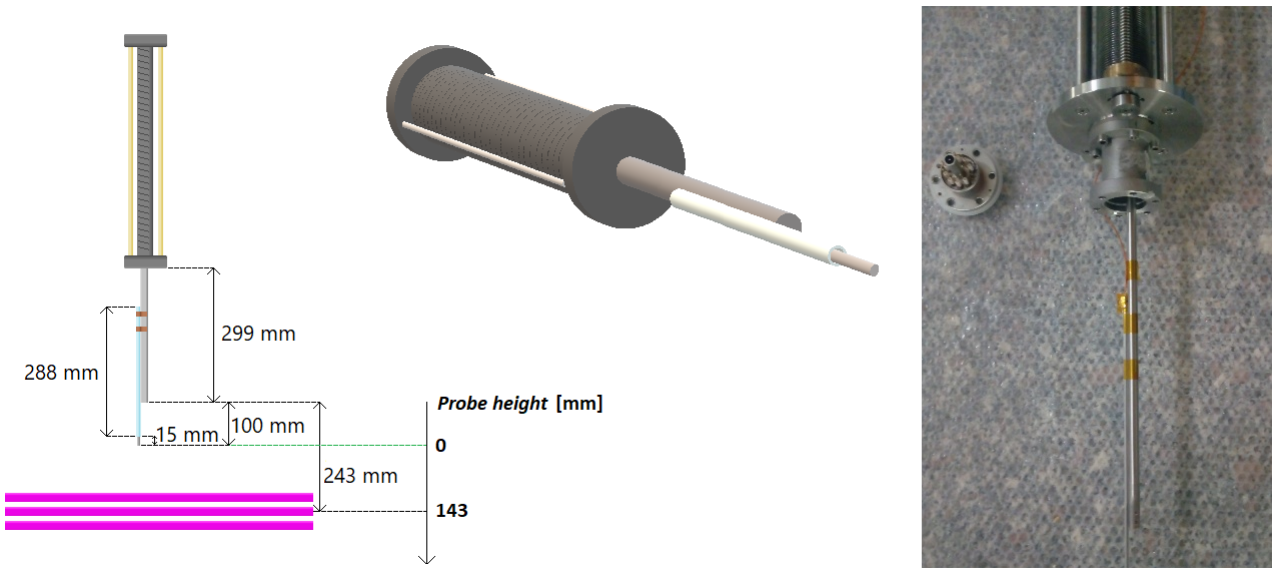

Figure 3.1: Langmuir probe.

When the probe is polarized with respect to the plasma, the region that surrounds the electrode is characterized by positive or negative charge excess: this region is called Debye sheath and is usually a few Debye lengths thick. The ideal working condition for the probe is when its radius is small compared to the Debye length.

Next table shows the Debye length λ_{De} for different n_{e} and T_e values:

	1 eV	5 eV	10 eV
$6.50 \times 10^{11} \mathrm{m}^{-3}$	9.22 mm	20.62 mm	29.16 mm
$5.05 \times 10^{12} \mathrm{m}^{-3}$	3.31 mm	7.40 mm	10.46 mm
$2.60 \times 10^{13} \mathrm{m}^{-3}$	1.46 mm	3.26 mm	4.61 mm

For $\mathrm{T}_e = 1\mathrm{eV}$ and $n_{\mathrm{e}} = 6.50 \times 10^{11}\ \mathrm{m}^{-3}$ λ_{De} is greater than 1 cm, so the probe effective surface might be greater than the beam area, which is 4 cm $\times$ 4 cm. In this situation the plasma conditions are no longer verified, since all the ions and electrons even outside the beam area are lost because they are collected by the probe.
For lower densities the ratio $\frac{a_{\mathrm{probe}}}{\lambda_{\mathrm{De}}}$ is greater than 1, so the probe might not work correctly. On the other hand, for higher densities the Debye length is shorter and the ratio is below 1: this is a better working condition for the probe.

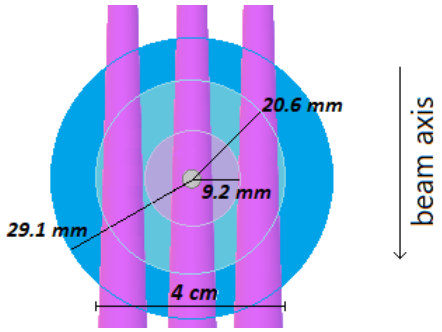

Figure 3.2: Different probe effective surfaces in comparison with the beam area.

3.2 Floating potential

In order to characterize the Debye sheath in presence of the beam, according to Figure 3.1 the probe height must be approximately 15 cm. This assumption was verified by measuring the floating potential V_{f}, i.e. the potential for which the collected current is zero, while moving the probe along the direction perpendicular to the beam.

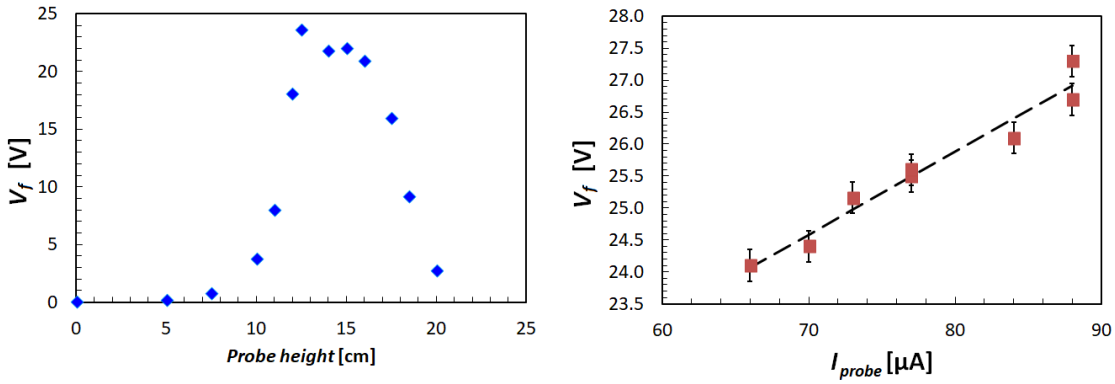

Figure 3.3: Floating potential data.

The probe was not polarized and the values of V_{f} were read on a tester connected to the probe itself. The first plot in Figure 3.3 shows the floating potential as a function of the probe height with constant beam current. The maximum value of V_{f} corresponds to a probe height between 14 cm and 15 cm.

The beam spatial density n_b has the same profile and its maximum corresponds to V_f^{max}. The beam is actually made of nine beamlets, but since the V_f measurements were made by moving the probe along one direction, only three beamlets can actually be observed (see Figure 3.4).

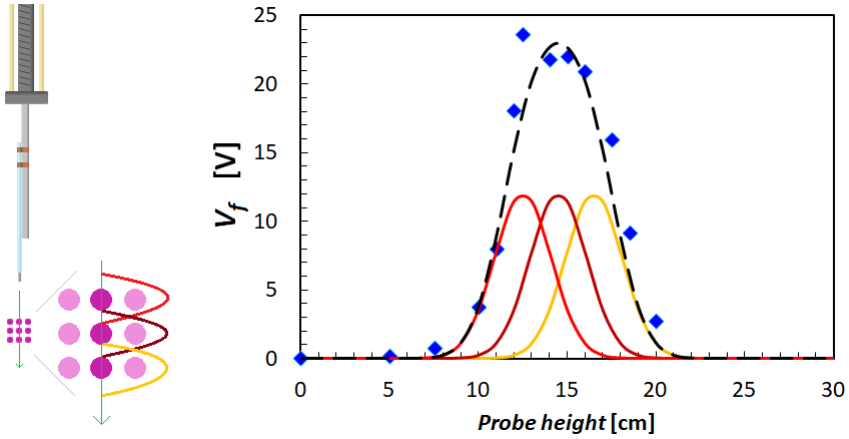

Figure 3.4: Beam density.

The total density can be obtained as the sum of three gaussian distributions, each one describing one of the three beamlets. The maximum value of this distribution is approximately 14.5 cm, so in order to characterize the sheath formation inside the beam region the probe must reach this position.

The second plot in Figure 3.3 shows some potential values measured at constant position while varying the beam current. By fitting the experimental points it is possible to obtain the floating potential for a fixed probe height as a function of the beam current.

m $[\frac{\mathrm{V}}{\mu\mathrm{A}}]$	q [V]
0.13 ± 0.01	15.5 ± 0.9

Table 3.1: Fit parameters for $V_f(I)$.

Table 3.1 shows the fit parameters, and the fit function is $V_f(I_{beam}) = mI_{beam} + q$. For example, if $I_{beam} = 100\mu A$ then $V_f = 28.5V$.

3.3 Preliminary measurements

If the probe is polarized with respect to the vessel, an I-V characteristic curve as the one shown in section 2.2 can be obtained.

A simple electrical scheme is shown in Figure 3.5. In this case $V_{probe} = V_{supply} + V_{shunt}$ and the probe current I_{probe} is given by the Ohm law:

$$I_{probe} = \frac{V_{probe}}{R_{shunt}} \tag{3.1}$$

The current signal was acquired with an oscilloscope.
In order to validate the results found in section 3.2, two different I-V curves were measured with two different probe heights, inside and outside the beam region.

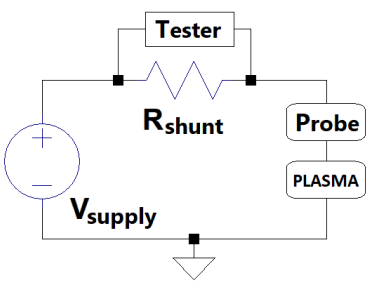

Figure 3.5: Electrical scheme.

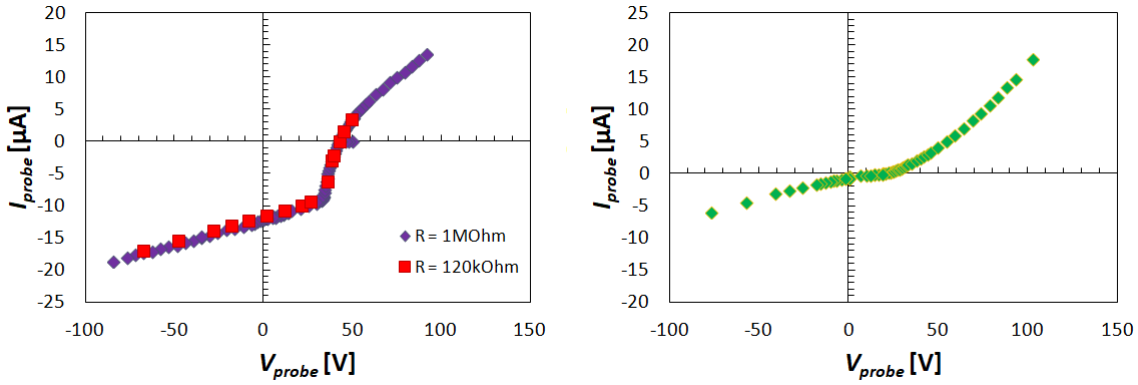

Figure 3.6: I-V characteristic curve inside and outside the beam.

The first plot in Figure 3.6 shows the I-V curve inside the beam, with $y = 14.5$ cm. For the purple series a resistance of $1M\Omega$ was used, while for the red series a resistance of $100k\Omega$ was used. The data trend doesn't change, so it is safe to say that the probe current does not depend on the resistance used in the circuit. The second plot shows another I-V curve measured outside the beam.

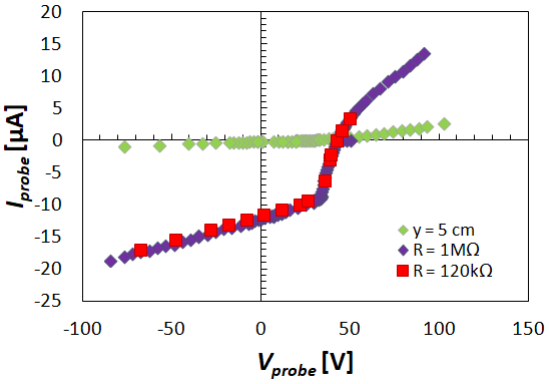

Figure 3.7: I-V characteristic curve comparison.

A comparison between both curves is shown in Figure 3.7. The current measured outside the beam region is significantly lower and it is instantly noticeable that the effect of the negative ion beam is to increase the ion saturation current.

3.4 Experimental I-V characteristics

In the next figures some dataset taken in different experimental conditions are shown. In particular, the changing parameters are the acceleration potential, V_{acc} (which is related to the beam energy U_{b}), the beam current and the vessel pressure, which is 0.3 mPa when the cryopump is off while is almost 30 mPa when the cryopump is on.

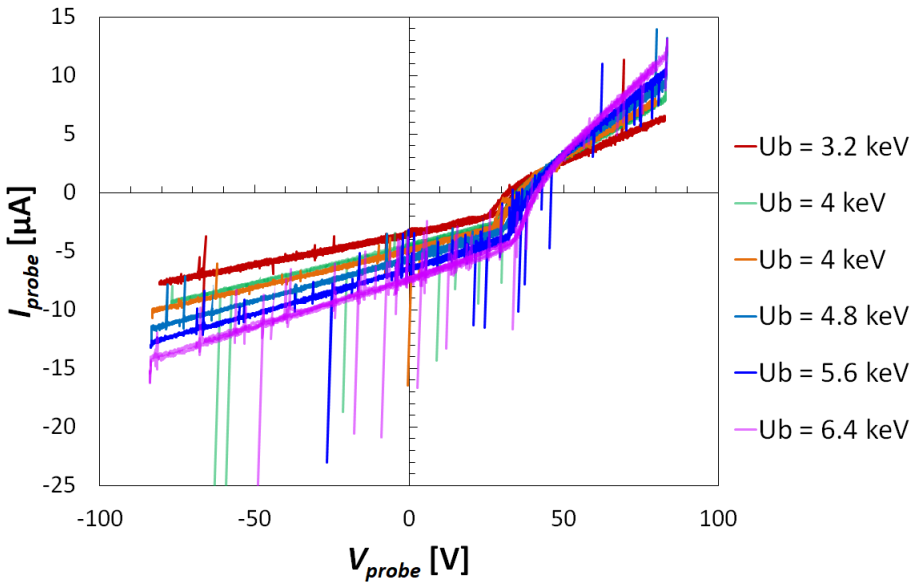

Figure 3.8: I-V characteristics without cryopump.

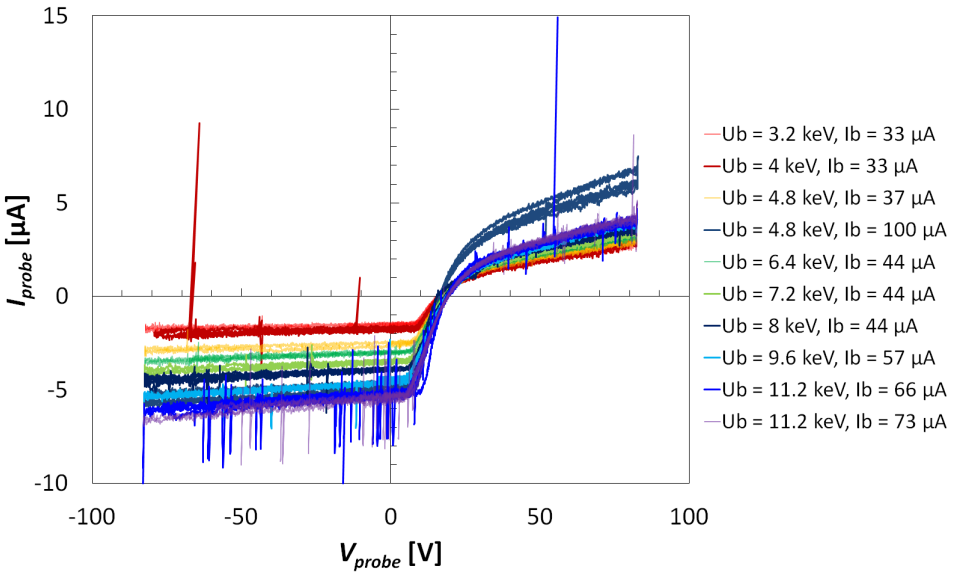

Figure 3.9: I-V characteristics with cryopump.

Chapter 4

Data analysis

All the experimental I-V curves were fitted with the theoretical expression for probe current defined in section 2.4. The most relevant quantity that can be obtained from the fit parameters is the positive ion density at sheath edge $n_{\mathrm{i,s}}$.

This chapter provides a brief description of the fit procedure and the final values for the fit parameters.

4.1 Fit parameters

In order to calculate each current contribution from section 2.1 it is necessary to know the spatial densities of all species.

Beam density

The beam density is constant and is defined as follows:

$$n_{\mathrm{beam}} = \frac{I^{tot}_{\mathrm{beam}}}{A_{\mathrm{beam}} e} \Big(\frac{m_{\mathrm{H^-}}}{2e} \Big)^{\frac{1}{2}} (U_{\mathrm{b}})^{-\frac{1}{2}} \tag{4.1}$$

It is possible to define $n_{\mathrm{H^0}}$, $n_{\mathrm{H^-}}$ and $n_{\mathrm{H^+}}$ in the same way:

$$n_{\mathrm{H^*}} = \frac{I^{tot}_{\mathrm{H^*}}}{A_{\mathrm{beam}} e} \Big(\frac{m_{\mathrm{H^i}}}{2e} \Big)^{\frac{1}{2}} (U_{\mathrm{b}})^{-\frac{1}{2}} \tag{4.2}$$

Plasma electrons density

The plasma electrons density at sheath edge $n_{\mathrm{e,s}}$ is assumed to be proportional to the total beam density n_{beam}:

$$n_{\mathrm{e,s}} = K n_{\mathrm{beam}} \tag{4.3}$$

where K is unknown and is a fit parameter. For electronegative plasma this parameter is usually replaced with $\alpha_{\mathrm{s}} = \frac{n_{\mathrm{H^-}}}{n_{\mathrm{e,s}}}$.

Secondary emitted electrons density

The secondary emitted electrons density at sheath edge is defined as follows:

$$n_{\mathrm{see,s}} = \frac{(\pi\gamma_{\mathrm{see}} + 1)I_{\mathrm{H^0}} + \pi\gamma_{\mathrm{see}}I_{\mathrm{H^-}}}{A_{\mathrm{beam}}e}\left(\frac{m_e}{2e}\right)^{\frac{1}{2}}(U_{\mathrm{see}} + V_{\mathrm{s}})^{-\frac{1}{2}} \tag{4.4}$$

where $U_{\mathrm{see}} = \frac{\mathrm{T_{see}}}{2}$ is the secondary emitted electrons initial energy and V_{s} is the potential drop at sheath edge. Both γ_{see} and $\mathrm{T_{see}}$ are unknown and are fit parameters.

Stripped electrons density

The stripped electrons density at sheath edge is defined as follows:

$$n_{\mathrm{se,s}} = \alpha_{\mathrm{strip}}\frac{I^{tot}_{\mathrm{beam}}}{A_{\mathrm{beam}}e}\left(\frac{m_e}{2e}\right)^{\frac{1}{2}}(U_{\mathrm{se}} + V_{\mathrm{s}})^{-\frac{1}{2}} \tag{4.5}$$

where $U_{\mathrm{se}} = \frac{m_e}{m_{\mathrm{H^-}}}$ is the stripped emitted electrons initial energy. α_{strip} is unknown and is a fit parameter.

Positive ions density

The positive ions density at sheath edge is obtained from quasi-neutrality:

$$n_{\mathrm{i,s}} = n_{\mathrm{H^-}} - n_{\mathrm{H^+}} + n_{\mathrm{e,s}} + n_{\mathrm{see,s}} + n_{\mathrm{se,s}} \tag{4.6}$$

Final set of fit parameters

The main fit parameters are $\mathrm{K} = \frac{n_{\mathrm{e,s}}}{n_{\mathrm{beam}}}$, the plasma potential V_{P}, the electron temperature $\mathrm{T_e}$, the secondary emitted electron temperature $\mathrm{T_{see}}$, the secondary emission coefficient γ_{see} and the electron stripping coefficient α_{strip}. The other quantities are indirectly defined through these parameters.

4.2 Positive ion saturation current

One of the major difficulties in the fitting procedure is the correct estimate of the ion saturation current slope. For the I-V curves measured without the cryopump the OML theory is not enough accurate since it underestimates the slope. This may be caused by an incorrect estimate of the sheath thickness, which with the OML theory is assumed to be equal to the impact parameter. To improve the analysis, a model for the sheath formation in the presence of a negative ion beam was developed (see Appendix C) and the final expression for sheath thickness is:

$$s = \lambda_{De}\sqrt{\frac{V - V_{\mathrm{P}}}{\mathrm{T}_e}}\sqrt{\frac{1 - \alpha_{\mathrm{s}}\gamma_{\mathrm{s}} - \alpha^{\mathrm{I}}_{\mathrm{s}}\gamma^{\mathrm{I}}_{\mathrm{s}} - \alpha^{\mathrm{II}}_{\mathrm{s}}\gamma^{\mathrm{II}}_{\mathrm{s}}}{1 + \alpha_{\mathrm{s}} + \alpha^{\mathrm{I}}_{\mathrm{s}} + \alpha^{\mathrm{II}}_{\mathrm{s}}}} \tag{4.7}$$

and the effective probe collecting surface is:

$$S^{+}_{\mathrm{eff}} = 2\pi(a + s)l + 2\pi(a + s)^2 \tag{4.8}$$

However, in this specific case the actual S_{eff}^{+} is 5 times smaller than the one provided by the sheath model.

For the I-V curves measured with the cryopump the OML theory is still not accurate since it overestimates the effective sheath thickness.
The slope of the ion saturation current is almost equal to zero, especially for lower beam energies U_{b}; the probe collecting surface was then assumed to be equal to the geometrical surface A_{probe}. This approximation causes a slight underestimation of the probe current for higher beam energies.

4.3 Data without cryopump

Three experimental I-V curves with different beam energies and currents with their respective fitted I-V curves are shown in the following figures.

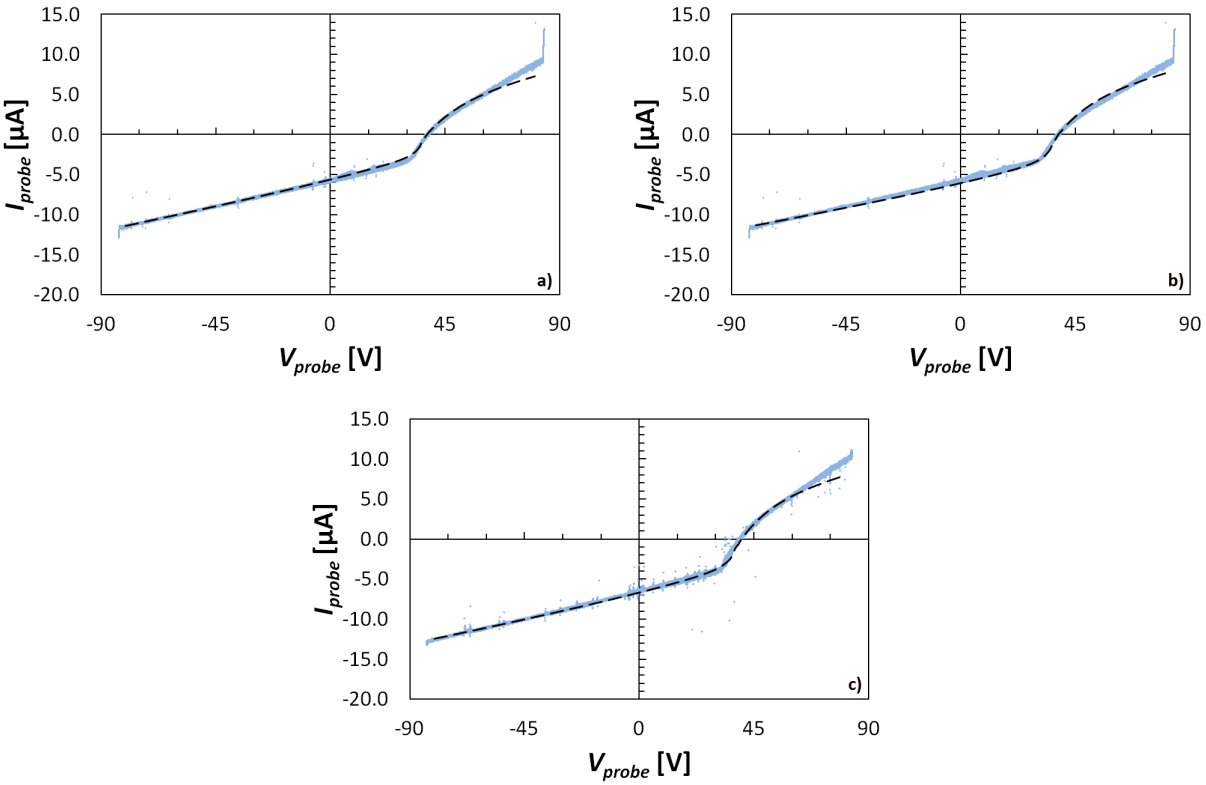

Figure 4.1: a): $U_{\text{b}} = 3.2$ keV,$I_{\text{CFC}} = 106\mu$A; b): $U_{\text{b}} = 4.8$ keV,$I_{\text{CFC}} = 106\mu$A; c): $U_{\text{b}} = 5.6$ keV,$I_{\text{CFC}} = 106\mu$A.

The fit parameters for all datasets are:

U_b [keV]	3.2	4	4.8	5.6	6.4
I_b [μA]	29	28	28	28	28
n_b [$\times 10^{11}$ m^{-3}]	1.46	1.26	1.15	1.06	0.97
n_{H^+} [$\times 10^{11}$ m^{-3}]	0.15	0.13	0.11	0.11	0.10
n_is [$\times 10^{11}$ m^{-3}]	4.92	5.12	5.58	5.95	6.71
n_es [$\times 10^{11}$ m^{-3}]	2.05	2.02	2.01	2.13	2.34
$n_\mathrm{see,s}$ [$\times 10^{11}$ m^{-3}]	0.90	1.02	1.15	1.26	1.58
$n_\mathrm{se,s}$ [$\times 10^{11}$ m^{-3}]	2.12	2.21	2.53	2.66	2.89
T$_e$ [eV]	2.6	3	3.1	3.4	3.6
T$_\mathrm{see}$ [eV]	9	8.5	8.5	8	8
γ_see [adim]	0.35	0.40	0.45	0.48	0.60
α_strip [adim]	1.45	1.75	2.2	2.5	2.9
K [adim]	1.40	1.60	1.75	2.00	2.35
V_p [V]	36	36	36	38	39

Table 4.1: Fit parameters for I-V characteristics without cryopump.

4.4 Data with cryopump

Two experimental I-V curves with different beam energies and currents with their respective fitted I-V curves are shown in the following figures:

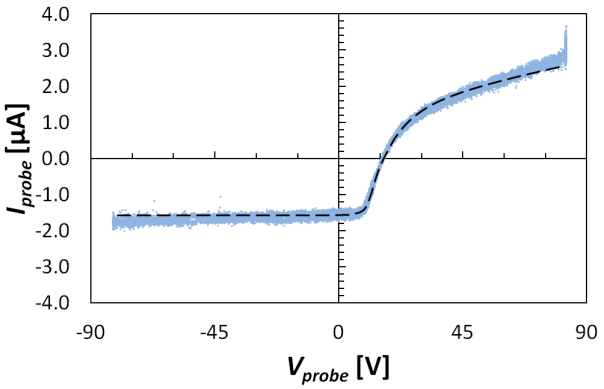

Figure 4.2: $U_\mathrm{b} = 3.2$ keV, $I_\mathrm{CFC} = 33\mu$A

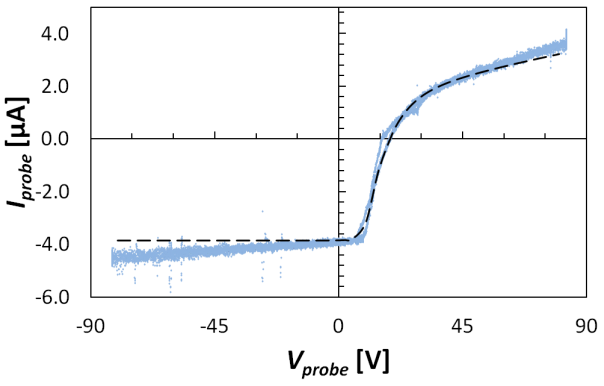

Figure 4.3: $U_\mathrm{b} = 6.4$ keV, $I_\mathrm{CFC} = 44\mu$A

The fit parameters for all datasets are:

U_b [keV]	3.2	4	4.8	6.4	7.2	8
I_b [μA]	30	30	34	40	40	40
n_b [$\times 10^{11}$ m^{-3}]	1.49	1.34	1.37	1.41	1.33	1.26
n_{H^-} [$\times 10^{11}$ m^{-3}]	0.56	0.50	0.51	0.63	0.60	0.57
n_is [$\times 10^{11}$ m^{-3}]	3.18	3.26	3.58	4.74	4.90	5.19
n_es [$\times 10^{11}$ m^{-3}]	0.21	0.21	0.22	0.35	0.40	0.44
$n_\mathrm{see,s}$ [$\times 10^{11}$ m^{-3}]	1.48	1.57	1.82	2.69	2.85	3.36
$n_\mathrm{se,s}$ [$\times 10^{11}$ m^{-3}]	0.57	0.60	0.57	0.51	0.53	0.50
T_e [eV]	3.5	3.5	3.5	2.5	2.5	2.5
T_see [eV]	6.5	6.5	6.5	6.5	6	6.5
γ_see [adim]	0.16	0.19	0.21	0.23	0.28	0.32
α_strip [adim]	0.38	0.45	0.42	0.36	0.40	0.40
K [adim]	0.14	0.16	0.16	0.25	0.30	0.35
V_p [V]	9.5	10	9.5	9.5	9	9

Table 4.2: Fit parameters for I-V characteristics with cryopump.

Chapter 5

Results

5.1 Fit parameters without cryopump

As can be seen in table 4.1, the positive ion density $n_{\mathrm{i,s}}$ is higher than all the other species and is 5 times higher than the beam density:

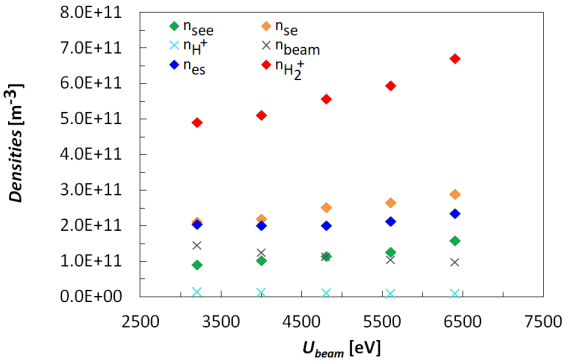

Figure 5.1: Densities - U_{b}.

The stripped electrons density is of the same order of magnitude as the plasma electrons density, while it is almost twice the secondary emitted electron density.

The electron temperature increases for higher beam energies and its mean value is approximately 3 eV. The parameter K is also greater for high extraction energies, as expected: if the beam is more energetic, the H_2^+ ionization process is favored so more plasma electrons and ions are produced.

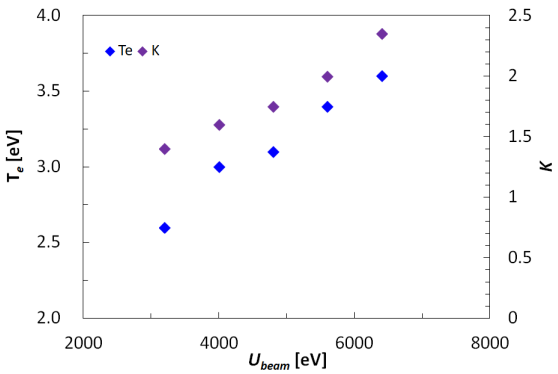

Figure 5.2: T_e, K - U_{b}.

The secondary emitted electron temperature decreases slightly. On the other hand, the secondary emission coefficient γ_{see} increases: this might be the reason why $n_{\mathrm{see,s}}$ is also larger for higher beam energies even if $\mathrm{T_{see}}$ is lower. The stripping coefficient α_{see} increases for higher beam energies.

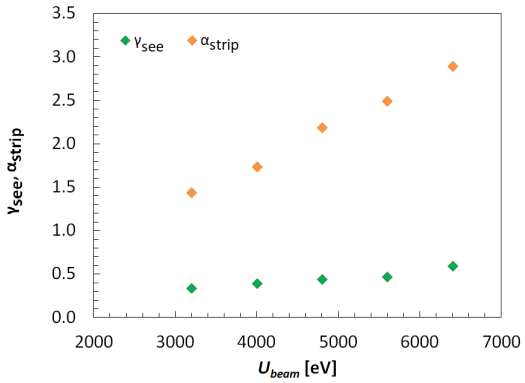

Figure 5.3: γ_{see},α_{strip} - U_{b}.

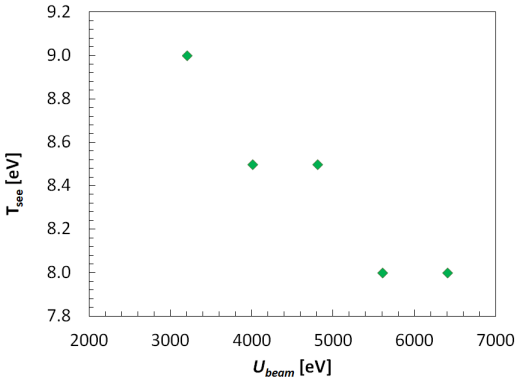

Figure 5.4: $\mathrm{T_{see}}$ - U_{b}.

The plasma potential is above 30 V and is even higher for increasing beam energies as expected, since the positive ion density is really high and increases for higher values of U_{b}.

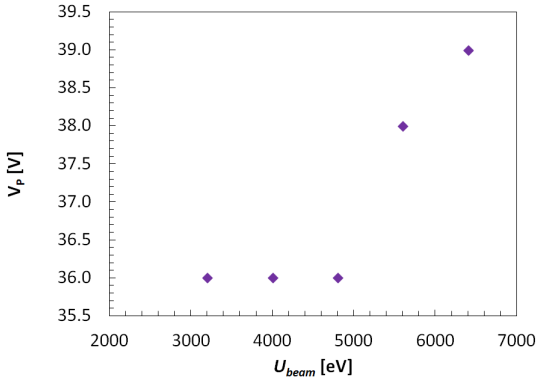

Figure 5.5: V_{P} - U_{b}.

5.2 Fit parameters with cryopump

As can be seen in table 4.2, even with the cryopump the positive ion density $n_{\mathrm{i,s}}$ is higher than all the other species. The stripped electrons density is still of the same order of magnitude as the plasma electrons density, while the secondary emitted electrons density is much higher with respect to the case without the cryopump.

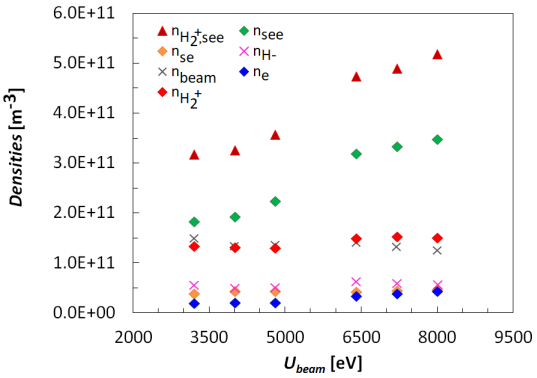

Figure 5.6: Densities - U_{b}.

Figure 5.6 shows also the positive ion density calculated without including the secondary emitted electrons in the quasi-neutrality equation. It would be an incorrect estimate since the quasi-neutrality criterion would not be satisfied, but it shows how considerable is the secondary emission contribution. The electron temperature decreases for higher beam energies and its mean value is 3 eV, while the K parameter also increases, as can be seen in the following figure:

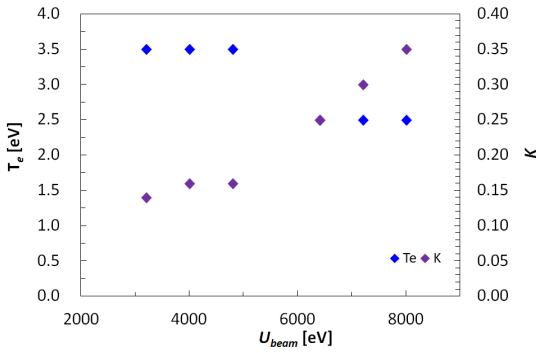

Figure 5.7: T_e, K - U_{b}.

The secondary electron emission coefficient increases slightly for higher beam energies while the stripping coefficient α_{strip} is approximately constant and its mean value is 0.25.

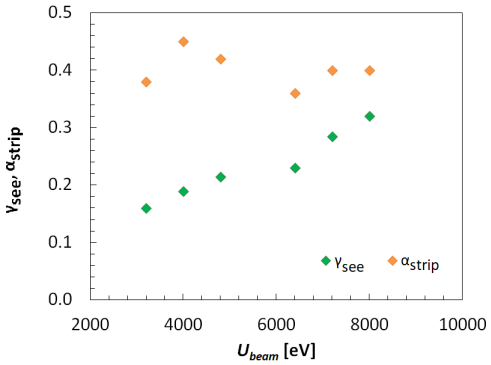

Figure 5.8: γ_{see}, α_{strip} - U_{b}

The secondary emitted electron temperature T_{see} is approximately constant, as can be seen in table 4.2, and its mean value is 6.4 eV. The plasma potential is also approximately constant and its mean value is 9.4 V, as can be seen in Figure 5.9:

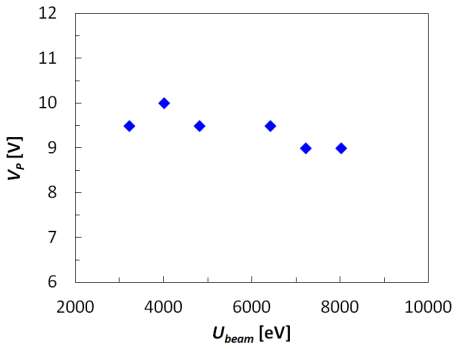

Figure 5.9: V_P - U_b

5.3 Beam energy and current influence

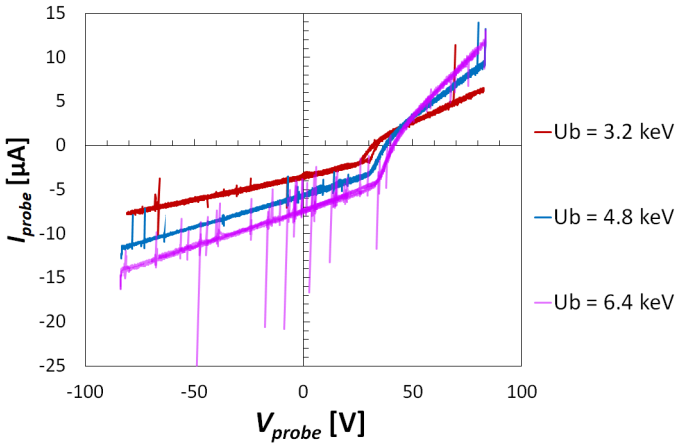

Figure 5.10: I-V curves without cryopump.

Figure 5.10 shows a comparison between three I-V characteristics measured without the cryopump already displayed in section 3.4. In this case the beam current was constant and its value was 110 μA.
The ion saturation current slope increases with U_b: this means that the presence of a constant density n_b has a non negligible influence on the sheath formation and its effect is greater when the beam has higher energy. The electron saturation current slope increases too, but this effect might be caused by both secondary emission and stripping.
Figure 5.11 shows some I-V characteristics with different values of U_b and I_b measured with the cryopump.

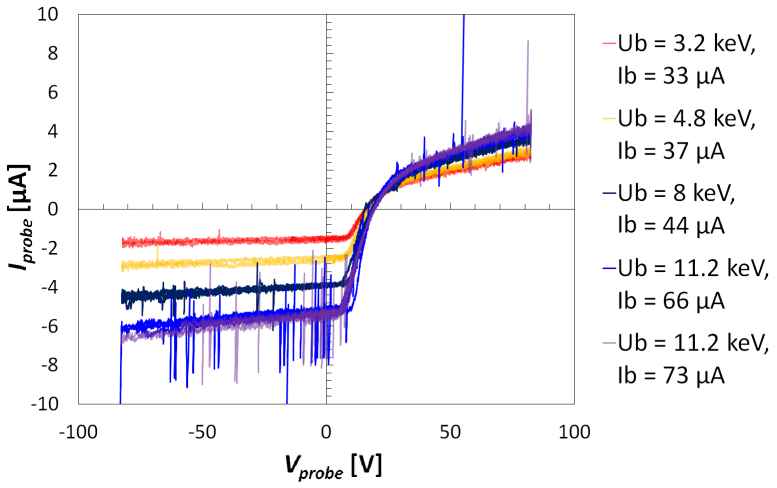

Figure 5.11: I-V curves with cryopump.

The beam current seems not to have a large influence, while the beam energy changes both the ion and electron saturation current slope.

5.3.1 Positive ion current slope and beam energy

Next figure shows how the ion saturation current slope changes for different beam energies when the cryopump is not working. It is difficult to analyze this aspect with these datasets since both the slope and current values are too low. However, this could be an interesting topic for future works.

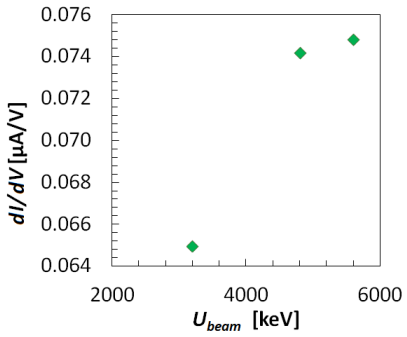

Figure 5.12: Ion saturation current slope - U_{beam}.

5.4 Secondary emission and electron stripping effect

Figure 5.10 shows two simulated I-V characteristics without cryopump both with and without the secondary emitted and stripped electrons:

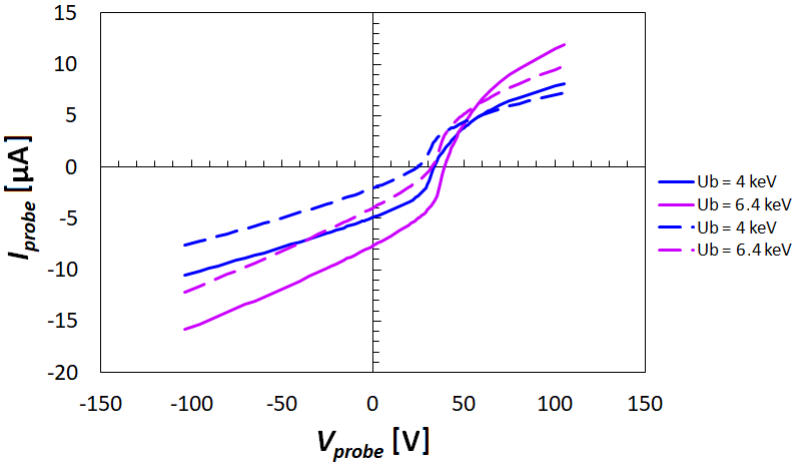

Figure 5.13: Simulation of I-V curves with and without secondary emitted and stripped electrons contributions, without cryopump.

The dashed lines refer to the curves without the electrons from secondary emission and stripping. The ion saturation current slope is the same but it is translated upwards, while the electron saturation current slope changes significantly.

The same effect can be observed on the characteristics with cryopump:

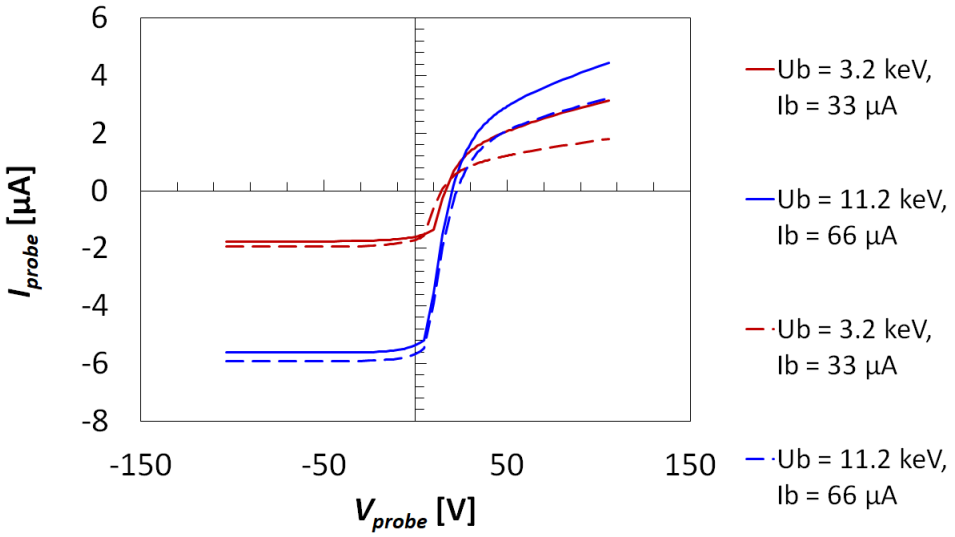

Figure 5.14: Simulation of I-V curves with and without secondary emitted and stripped electrons contributions, with cryopump.

This comparison shows that the two current contributions I_{see} and I_{se} are not negligible, especially when the cryopump is working. Moreover, they may be the reason why the positive ion current is comparable with the electron current. In fact, as shown in Figure 5.15, in a simulated I-V curve with only plasma ions and electrons the ion current is usually smaller than the electron current because the ions have lower mobility.

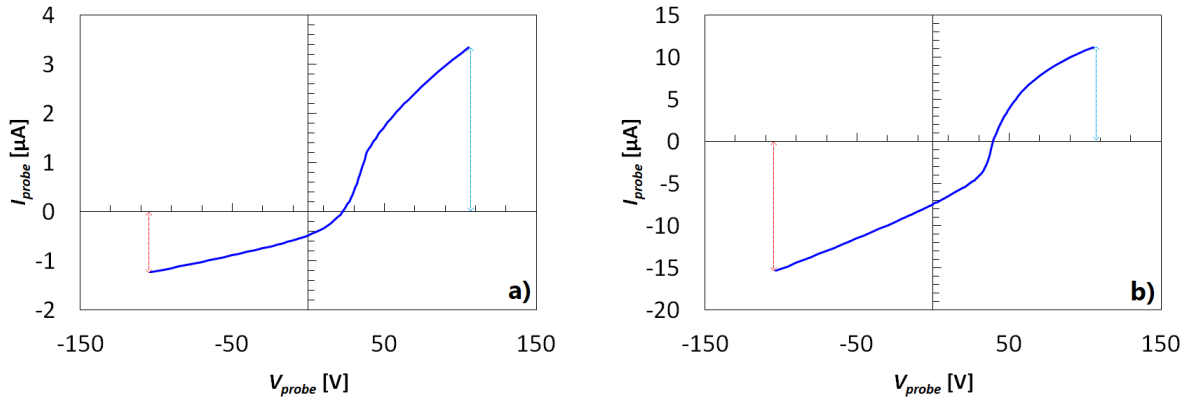

Figure 5.15: Simulation of two I-V curves with and without the beam.

The beam presence brings secondary emission, which amplifies the ion current. This effect is visible in almost all the measured I-V curves, independently from the operation of the cryopump.

5.5 Cryopump effect

Both plasma ion and electron densities are higher when the cryopump is not working: $n_{e,s}$ is almost two orders of magnitudes higher, while the ions are approximately twice the density measured with the cryopump. The stripped electrons density is also higher when the cryopump is not working.
This may be caused by the background gas density variation: when the cryopump is not working, this density is almost one order of magnitude higher, so both the ionization and the stripping processes are favored. When the cryopump is working the background gas has a lower density, so the effects of secondary emission are more conspicuous.

By comparing the parameters from tables 4.1 and 4.2 it is possible to observe that the electron temperature is not much different, while T_{see} is higher when the cryopump is working.
The secondary emission coefficient is of the same order of magnitude in both cases, while the stripping coefficient is remarkably higher when the cryopump is not working.

Next figure shows two I-V characteristics with and without cryopump measured with the same beam energy and current:

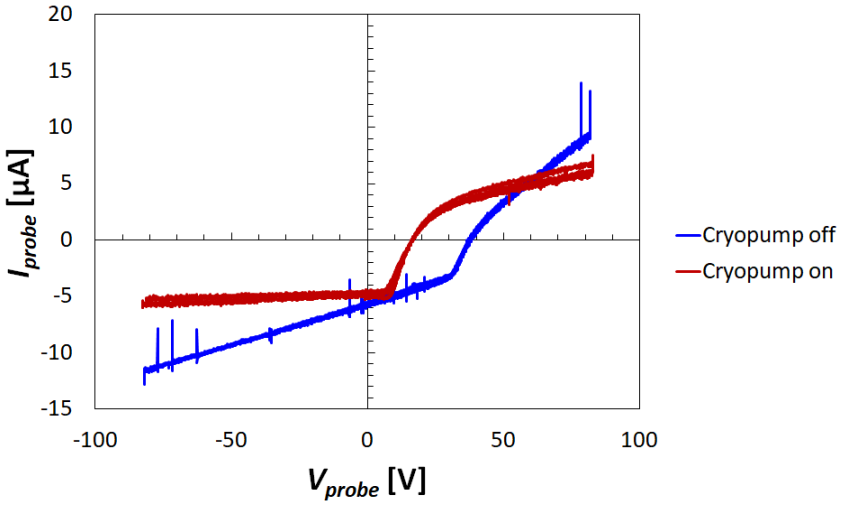

Figure 5.16: I-V curves with and without cryopump.

Both the ion and the electron saturation current slopes are smaller when the cryopump is on, since both $n_{i,s}$ and $n_{e,s}$ are smaller.

Conclusions

The aim of this thesis work was the investigation of the NIO1 beam propagation, with a particular focus on the space charge compensation phenomenon. The chosen diagnostic instrument was a single Langmuir probe, which provided some fundamental information such as densities and temperatures of the species considered.
It was possible to understand how the beam presence influences both the space charge density and the sheath formation in different experimental conditions.

The first experimental evidence is that the H_2^+ density increases for higher beam energies, independently of the cryopump operation. However, the cryopump effect is visible by analyzing the electron densities: in fact, when the cryopump is operating the H_2^+ increase is mainly due to secondary emission, whose influence is even larger for higher beam energies. If the background gas density is too low the secondary emission may prevail on all other contributions: this would not be helpful for the investigation of space charge compensation since these conditions are strictly related to the probe presence.

On the other hand, when the cryopump is not operating the secondary emission effect is less visible but still not negligible. In this case the H_2^+ density increase is mainly due to electron stripping, and also plasma electrons have higher density with respect to the case with cryopump.

According to these results, in order to investigate space charge compensation with a Langmuir probe it might be useful to operate with higher background gas densities, since the probe itself should not excessively perturbate the plasma. However, if the H_2 density is higher the beam energy should also increase, otherwise the beam would be dispersed because of neutralization.

Another experimental evidence is the presence of the emitted electrons, which can be immediately deduced from the I-V characteristics since the ion current is comparable or even larger than the electron current.

One main aspect that has been investigated in this work is the ion saturation current slope, since it is fundamental to understand the I-V characteristics, especially the ones measured when the cryopump was not operating. In this case the OML theory was not sufficiently accurate to determine the sheath thickness, so a theoretical model was developed to achieve a better estimate for the sheath dimension. However, the predicted result was not completely exact and phenomenologically it was necessary to reduce the obtained value for the effective probe collecting surface in order to achieve a better fit.

On the other hand, in the I-V characteristics measured when the cryopump was operating the ion current slope is much lower and is almost equal to zero for low beam energies: this again confirms that the secondary emission current dominates over the other current contributions. In this case both the OML theory and the sheath model were not accurate.
This might be considered a border case in which the plasma is almost totally made of positive ions and secondary emitted electrons, so it might be necessary to improve the sheath model or even to develop a new model with different hypothesis.

Regarding the sheath model, it can be improved also by including the "virtual cathode" effect: if the probe potential is lower with respect to the plasma potential and the emitted electron flux is greater than the space charge limit, the emitted electron current reaches its maximum value and it is not

possible to extract more electrons from the probe surface even with higher beam energies because a virtual cathode has formed in the sheath region. As a consequence, the positive ions are retarded and the collected ion current should decrease. Moreover, all the densities at sheath edge might have different ratios.

An interesting experimental evidence is that the ion saturation current slope increases for higher beam energies, with constant background gas density. This effect is more visible in the I-V characteristics measured without the cryopump and might be further investigated in order to quantitatively describe this relation, since in this work only a qualitative trend could be provided.

Another aspect that can be improved is the electron saturation current slope estimation for high probe voltages: the real value is higher than the estimated one, especially when the cryopump is not operating.

Understanding space charge compensation is fundamental for MITICA experiment and to develop highly efficient beam injectors for the ITER reactor. As seen in this work, both the background gas density and the beam energy influence the beam propagation: for a given beam energy, a higher background gas density provides a larger amount of both plasma positive ions, useful as they compensate for the beam space charge, and electrons, but it may cause beam dispersion because of neutralization within a short distance. On the other hand, for a given background gas density, a higher beam energy allows the H^- ions to propagate for greater distances.

On this basis, it might be helpful to understand if there is an optimal value of background gas density for a given beam energy and, if this value exists, how it changes for varying beam energies. In this conditions it should be possible to obtain the maximum amount of positive ions, which would help to keep the beam collimated, while restraining the neutralization effect so that the beam would not be immediately dispersed.

Regarding the continuation of the activities, it might be useful to repeat the same experiment with a single Langmuir probe with smaller radius, even if the collected current would be significantly lower. In this case the plasma perturbation should be reduced and it might be easier to characterize spatial charge with lower background gas densities.

As a final remark, it must be noted that the measurements were carried out in a very challenging condition, with the NIO1 negative ion beam performing very poorely, both with respect to past NIO1 operations and to any other negative ion beam experiment. In fact, with the beam current in the range of μA, the beam plasma density was 10^{12} m^{-3} or below.
In some conditions, the collected current could approach the total secondary charges produced by the beam. For this reason, it was very hard to perform the probe measurements and it was not possible to operate in a condition in which the probe-induced perturbation was minimized.

Given this background, another way to improve this investigation is to operate with higher extraction energies: in this case, even with higher H_2 densities, the beam should propagate for longer distances and consequently reach the probe. In this case the secondary emission contribution might be larger and as a consequence the positive ion density might be greater.

It would also be useful to combine this diagnostic method with different ones, since the comparison of data coming from different diagnostics would certainly help to achieve a deeper understanding of all considered phenomena. In particular, it would be interesting to investigate how densities change in both directions perpendicular to the beam axis.

Appendix A: OML Theory

When the bias between the probe potential and the plasma potential is not zero, the charged particles are attracted by the probe and they orbit around it, so the effective probe collecting surface increases because of these orbital effects.

The **O**rbital **M**otion **L**imited Theory provides a way to estimate the effective collecting surface and it is applicable when the ratio $\frac{a_{\text{probe}}}{\lambda_{\text{De}}}$ is less then 1. In this theory the sheath effect is neglected.

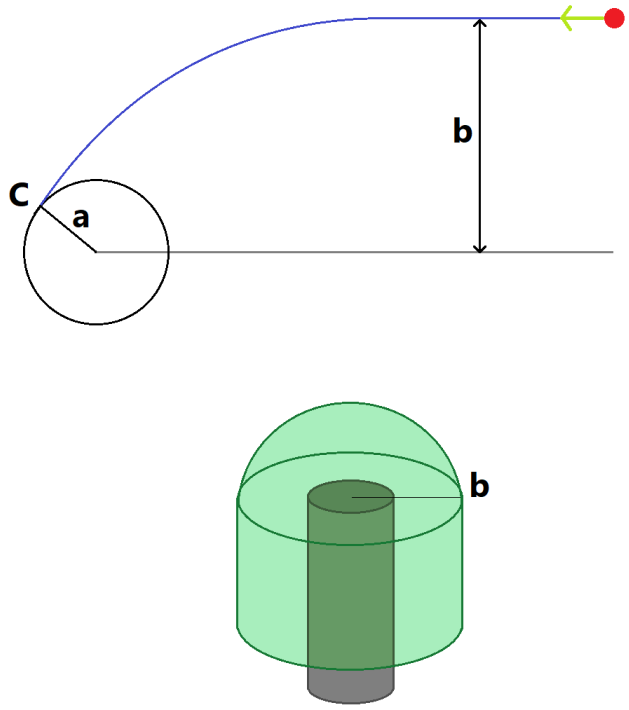

Application of conservation laws and effective probe surface

When a particle approaches the probe it orbits around it because of Coulomb interaction. There is an *impact parameter* b which can be obtained from the conservation laws of energy and angular momentum:

$$m_{e^-} b v = m_{e^-} r v_C$$

$$\frac{1}{2} m_{e^-} v^2 - e V_p = \frac{1}{2} m_{e^-} {v_C}^2 - eV$$

In point C the particle velocity has no radial component. When r is equal to the probe radius the maximum impact parameter b_{max} is obtained: if $b > b_{max}$, the particle will not be collected.

$$b_{max} = a_{probe} \sqrt{1 + \frac{2e(V_c - V_0)}{m {v_0}^2}}$$

and the effective collecting surface is given by:

$$S_{eff} = 2\pi {b_{max}}^2 + 2\pi b_{max} l$$

OML for stripped electrons

The OML effect is essential for good estimate of the stripped electron current I_{se}, as can be seen in the following figure:

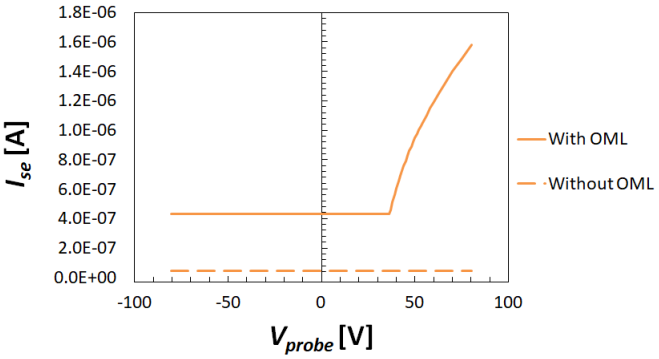

I_{se} currents with and without OML correction

OML for secondary emitted electrons

In this case the OML effect is not as prevailing as for the positive ions and stripped electrons, but it is not negligible:

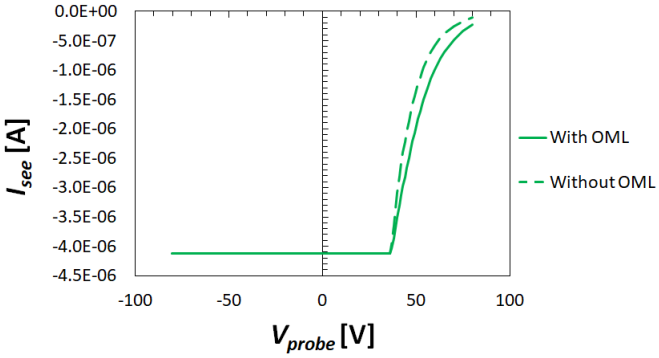

I_{see} current with and without OML correction

OML for H^- ions

The beam current is supposed to be constant in the sheath region. This assumption is correct because the H^- ions are too fast to be affected by the probe attraction, so the OML theory correction is negligible:

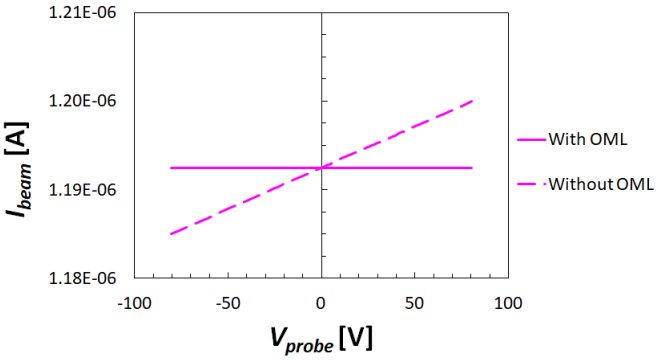

I_{b} current with and without OML correction

Appendix B: Sheath model

When the potential bias between the probe and the plasma is not equal to zero, the probe surface actually increases because of the orbital motion of particles and because of the Debye sheath, which is a few Debye lengths thick. There are different theories that describe this effect on the ion saturation current (Child-Langmuir theory, OML theory, ABR theory, Lafambroise theory) but none of them takes account of an energetic ion beam.

In order to determine the effective ion current collected by the probe it is necessary to analyze how the Bohm velocity for positive ions and the sheath dimension change according to other plasma parameters such as the temperatures and densities of other species, the beam energy and the beam current.
To provide all these information, an analytical model for the sheath based on the article by Bredin [4] has been developed, as explained in this appendix. This model describes the sheath until the formation of the virtual cathode.

In the next figure the sheath potential depending on the distance from probe surface is shown:

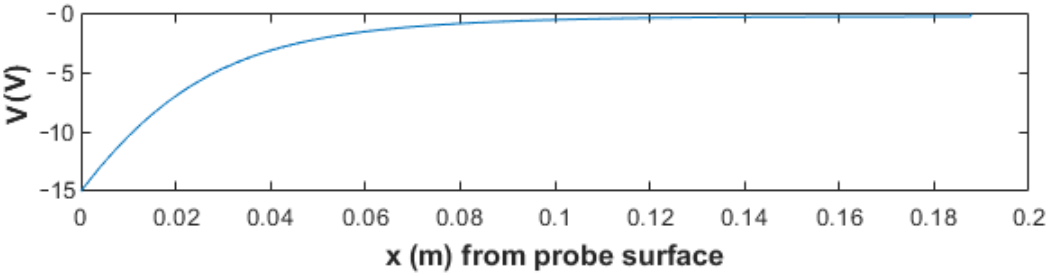

Sheath potential

The potential V is measured from the sheath edge and is a negative quantity and the probe potential is $-V_p$, where V_p is a positive quantity. In order to obtain the sheath thickness the Gauss law in cylindrical coordinates and the positive ion energy conservation were used:

$$\frac{1}{r}\left(r\frac{\partial E(r)}{\partial r}\right) = \frac{e}{\epsilon_0} n_{tot}$$

$$\frac{1}{2} m_{H_2^+} u(r)^2 = -eV$$

Where V is the potential drop in the sheath. By differentiating the second equation:

$$\frac{\partial u(r)}{\partial r} = \frac{eE(r)}{m_{H_2^+} u(r)}$$

This equation and the first one can then be solved numerically to obtain the sheath thickness as a function of the potential drop of the sheath itself. In this case, the total density at sheath edge is given by the following equation:

$$n_{\mathrm{tot}} = n_{\mathrm{H^-}} - n_{\mathrm{H^+}} - n_{\mathrm{i,s}} + n_{\mathrm{e,s}} + n_{\mathrm{see,s}} + n_{\mathrm{se,s}}$$

The densities are defined as follows:

$$n_{\mathrm{H^-}} = \frac{I_{\mathrm{H^-}}}{eA_{\mathrm{beam}}v_{\mathrm{b}}} = \frac{I_{\mathrm{H^-}}}{eA_{\mathrm{beam}}}\left(\frac{m_{\mathrm{H^-}}}{2e}\right)^{\frac{1}{2}}(U_{\mathrm{b}} + V)^{-\frac{1}{2}}$$

$$n_{\mathrm{H^+}} = \frac{I_{\mathrm{H^+}}}{eA_{\mathrm{beam}}v_{\mathrm{b}}} = \frac{I_{\mathrm{H^+}}}{eA_{\mathrm{beam}}}\left(\frac{m_{\mathrm{H^+}}}{2e}\right)^{\frac{1}{2}}(U_{\mathrm{b}} + V)^{-\frac{1}{2}}$$

$$n_{\mathrm{i}}(r) = \frac{J_0}{eu(r)}$$

where J_0 is the ion current at the sheath edge.

$$n_{\mathrm{e}} = n_{e,s}e^{\frac{V}{\mathrm{T}_e}}$$

$$n_{\mathrm{see}} = \frac{(\pi\gamma_{\mathrm{see}} + 1)I_{\mathrm{H^0}} + \pi\gamma_{\mathrm{see}}I_{\mathrm{H^-}}}{A_{\mathrm{beam}}e}\left(\frac{m_e}{2e}\right)^{\frac{1}{2}}(U_{\mathrm{see}} + V)^{-\frac{1}{2}}$$

$$n_{\mathrm{se}} = \alpha_{\mathrm{strip}}\frac{I^{tot}_{\mathrm{beam}}}{A_{\mathrm{beam}}e}\left(\frac{m_e}{2e}\right)^{\frac{1}{2}}(U_{\mathrm{se}} + V)^{-\frac{1}{2}}$$

The solution of the system gives the sheath thickness as a function of the sheath potential drop:

$$s = \sqrt{\frac{V - V_{\mathrm{P}}}{\mathrm{T}_e}}\sqrt{\frac{1 - \alpha_{\mathrm{s}}\gamma_{\mathrm{s}} - \alpha^{\mathrm{I}}_{\mathrm{s}}\gamma^{\mathrm{I}}_{\mathrm{s}} - \alpha^{\mathrm{II}}_{\mathrm{s}}\gamma^{\mathrm{II}}_{\mathrm{s}}}{1 + \alpha_{\mathrm{s}} + \alpha^{\mathrm{I}}_{\mathrm{s}} + \alpha^{\mathrm{II}}_{\mathrm{s}}}}$$

where:

$$\alpha_s = \frac{n_{\mathrm{H^-}}}{n_{\mathrm{e,s}}}, \alpha^{\mathrm{I}}_s = \frac{n_{\mathrm{see,s}}}{n_{\mathrm{e,s}}}, \alpha^{\mathrm{II}}_s = \frac{n_{\mathrm{se,s}}}{n_{\mathrm{e,s}}}$$

$$\gamma_s = \frac{\mathrm{T}_e}{2U_{\mathrm{b}}}, \gamma^{\mathrm{I}}_s = \frac{\mathrm{T}_e}{2(U_{\mathrm{see}} + V_{\mathrm{S}})}, \gamma^{\mathrm{II}}_s = \frac{\mathrm{T}_e}{2(U_{\mathrm{se}} + V_{\mathrm{S}})}$$

The effective probe collecting surface is:

$$S_{\mathrm{eff}} = 2\pi(a + s)l + 2\pi(a + s)^2$$

Normalization factor

The normalization factor $\sqrt{\frac{1-\alpha_s\gamma_s-\alpha_s^I\gamma_s^I-\alpha_s^{II}\gamma_s^{II}}{1+\alpha_s+\alpha_s^I+\alpha_s^{II}}}$ was obtained by applying the Amemiya criterion [5], which requires quasi-neutrality at sheath edge and that the derivative of the total space charge density is zero at the sheath edge $\frac{dn}{dV} = 0_{[V=0]}$. In this case the n_{H^+} density is negligible and it won't be considered.

$$\frac{dn_{\mathrm{tot}}}{dV} = \frac{n_{\mathrm{i,s}}}{2V_0} - \frac{n_{\mathrm{e,s}}}{T_e} + \frac{j_{\mathrm{b}}^{tot}}{e}\left(\frac{M_b}{e}\right)^{\frac{1}{2}}(2U_{\mathrm{b}})^{-\frac{3}{2}} + \frac{n_{\mathrm{see,s}}}{2(U_{\mathrm{see}}+V_{\mathrm{S}})} + \frac{n_{\mathrm{se,s}}}{2(U_{\mathrm{se}}+V_{\mathrm{S}})} = 0$$

$$V_0 = \frac{n_{i0}}{2}\left\{\frac{n_{e0}}{T_e} - \frac{j_b}{e}\left(\frac{M_b}{e}\right)^{\frac{1}{2}}(2U_b)^{-\frac{3}{2}} - \frac{n_{\mathrm{see,s}}}{2(U_{\mathrm{see}}+V_{\mathrm{S}})} - \frac{n_{\mathrm{se,s}}}{2(U_{\mathrm{se}}+V_{\mathrm{S}})}\right\}^{-1}$$

$$V_0 = \frac{T_e}{2}\frac{1+\frac{n_{H^-}}{n_{e,s}}+\frac{n_{\mathrm{see,s}}}{n_{\mathrm{e,s}}}+\frac{n_{\mathrm{se,s}}}{n_{\mathrm{e,s}}}}{1-\frac{n_{H^-}}{n_{e,s}}\frac{T_e}{2U_{\mathrm{b}}}-\frac{n_{\mathrm{see,s}}}{n_{e,s}}\frac{T_e}{2(U_{\mathrm{see}}+V_{\mathrm{S}})}-\frac{n_{\mathrm{se,s}}}{n_{e,s}}\frac{T_e}{2(U_{\mathrm{se}}+V_{\mathrm{S}})}}$$

By substituting the previous definitions:

$$V_0 = \frac{T_e}{2}\frac{1+\alpha_s+\alpha_s^I+\alpha_s^{II}}{1-\alpha_s\gamma_s-\alpha_s^I\gamma_s^I-\alpha_s^{II}\gamma_s^{II}}$$

To include also the n_{H^+} density it is necessary to define another parameter which describes the density ratio between H^+ ions and plasma electrons.

Sheath model without secondary emission and electron stripping

If the secondary emission and electron stripping contributions are not considered $\alpha_s^I = \alpha_s^{II} = 0$ and $\gamma_s^I = \gamma_s^{II} = 0$. If these conditions are verified it is easier to show the efficiency of the normalization factor:

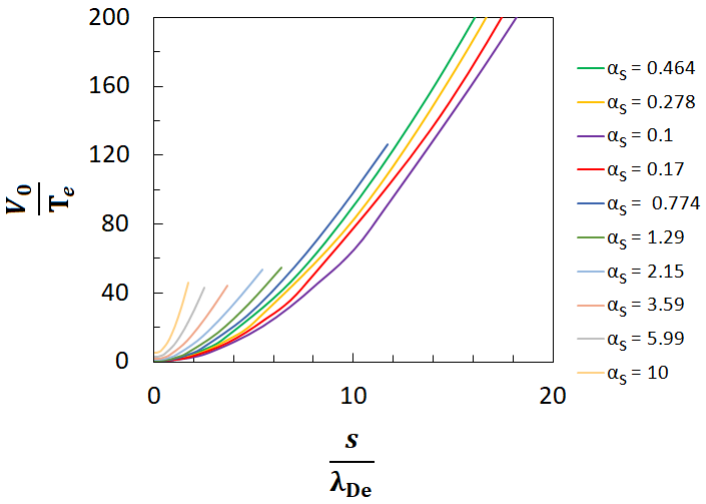

Sheath thickness as a function of the potential drop V_0.

For higher values of α_s the plasma electron density is lower and the sheath is less thick. Next figure shows the same curves with the normalization factor:

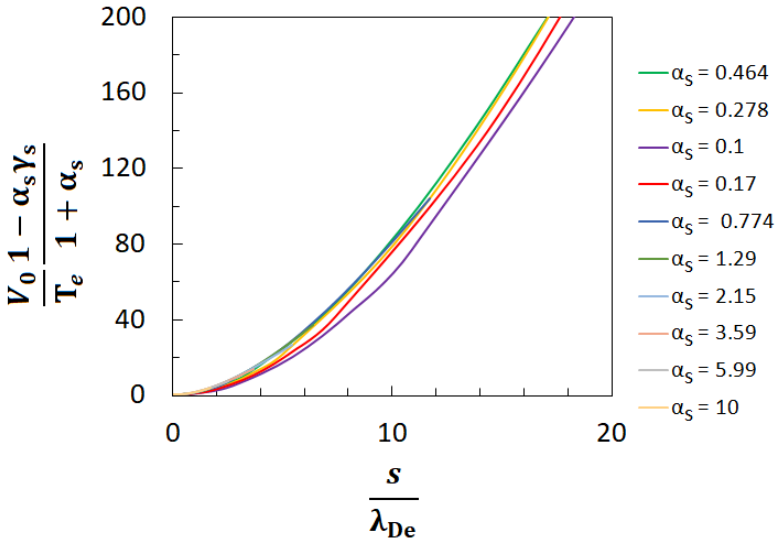

Sheath thickness as a function of the normalized potential drop V_0.

This normalization works better for lower values of $\frac{V_0}{T_e}$. From the normalized curves it is possible to obtain the sheath thickness as a function of α_s:

$$s = \lambda_{De} e^{-\frac{a(\alpha_s)}{2}} \sqrt{\frac{V_0}{T_e}\frac{1-\alpha_s\gamma_s}{1+\alpha_s}}$$

where $a(\alpha_s) = (-0.0031\alpha_s^2 + 0.0581\alpha_s - 0.597)^{-1}$.

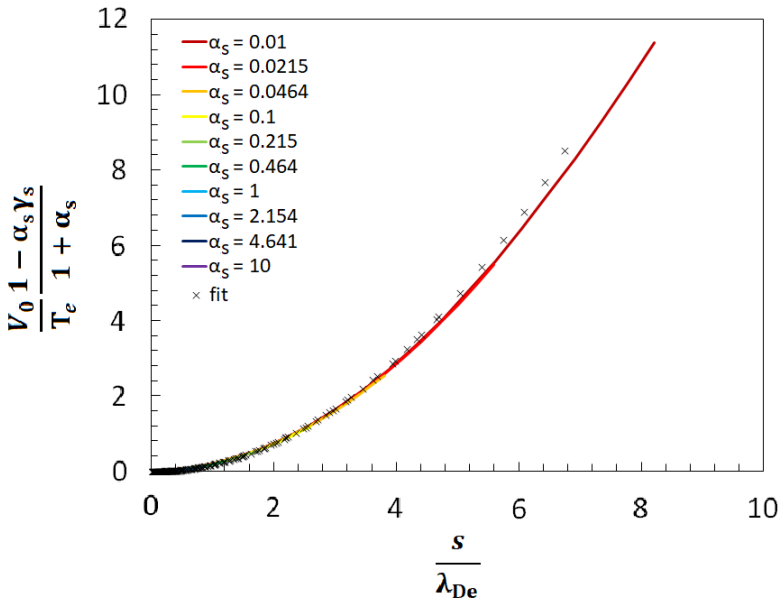

Sheath thickness as a function of the normalized potential drop V_0 compared with the fit function.

For $\alpha_s = 0$ the expression is:

$$s = 5.33\lambda_{De}\sqrt{\frac{V_0}{T_e}}$$

Next figure shows the same expression in cartesian coordinates in different situations, compared with the Child-Langmuir expression:

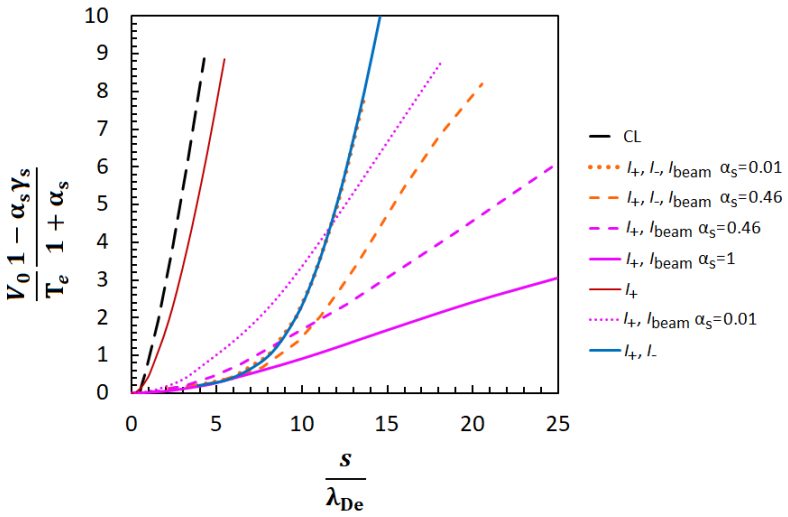

Potential drop as a function of the sheath thickness.

The sheath thickness increases in the presence of the beam. For higher values of α_s this effect is more visible because the beam density is much higher than the plasma electron density. This figure also explains why the OML theory, whose basic hypothesis are not different from the Child-Langmuir hypothesis[9], underestimates the sheath thickness for the I-V curves measured without the cryopump.

Appendix C: Modified Bohm velocity

Positive ions reach the sheath edge with a speed given by Bohm velocity, which is generally defined as:

$$u_{\mathrm{Bohm}} = \sqrt{\frac{e\mathrm{T}_e}{m_{\mathrm{H}_2^+}}}$$

However, as shown by Bredin [4], this expression is no longer valid for electronegative plasmas where electrons and both positive and negative ions are considered. This result is in agreement with the Amemiya criterion for the positive ion initial energy V_0, which requires the derivative of the total space charge density with respect to the potential V to be zero at sheath edge. If an ion beam is present together with plasma electrons and positive ions, the new expression for the modified Bohm velocity can be obtained by applying the Amemiya criterion:

$$u^*_{\mathrm{Bohm}} = \sqrt{\frac{e\mathrm{T}_e}{m_{\mathrm{H}_2^+}}} \sqrt{\frac{1 + \alpha_{\mathrm{s}} + \alpha_{\mathrm{s}}^{\mathrm{I}} + \alpha_{\mathrm{s}}^{\mathrm{II}}}{1 - \alpha_{\mathrm{s}}\gamma_{\mathrm{s}} - \alpha_{\mathrm{s}}^{\mathrm{I}}\gamma_{\mathrm{s}}^{\mathrm{I}} - \alpha_{\mathrm{s}}^{\mathrm{II}}\gamma_{\mathrm{s}}^{\mathrm{II}}}}$$

References

- [1] E. Sartori et al., *Improving the transported negative ion beam current in NIO1* (Submitted to AIP Conference Proceedings, 2018).
- [2] P. Chabert, N. Braithwaite, *Physics of Radio-Frequency Plasmas* (Cambridge University Press, Cambridge, 2011).
- [3] O. Auciello, D. L. Flamm, N. Hershkowitz, *Plasma-Materials Interactions* vol.1, chapter 3 (Academic Press INC, San Diego, 1989)
- [4] J. Bredin, P. Chabert, A. Aanesland, *Langmuir probe analysis in electronegative plasmas*, Physics of Plasmas 21, 123502 (2014); doi: 10.1063/1.4903328
- [5] H. Amemiya, B. M. Annaratone, J. E. Allen, *The double sheath associated with electron emission into a plasma containing negative ions*, J. Plasma Physics (1998), vol. 60, part 1, *pp* 81-93 (Cambridge University Press, 1998).
- [6] ITER Organization, https://*www.iter.org*/.
- [7] M. Cavenago et al., *First experiments with the negative ion source NIO1*, Review of Scientific Instruments 87, 02B320 (2016); doi: 10.1063/1.4932616
- [7] M. Cavenago et al., *Improvements of the versatile multiaperture negative ion source NIO1*, AIP Conference Proceedings 1869, 030007 (2017); doi: 10.1063/1.4995727
- [8] M. Kikuchi et al., *Fusion Physics* (International Atomic Energy Agency, Vienna, 2012).
- [9] M. A. Lieberman, A. J. Lichtenberg, *Principles of Plasma discharges and Materials processing* (John Wiley & Sons, INC, Hoboken, New Jersey, 2005).